

KEK Report 2006-2

July 2006

A

Stainless-steel X-band High Power RF Load with Low Surface Field

A. Lounine, T. Higo, N. Kudo and K. Watanabe



High Energy Accelerator Research Organization

+

© High Energy Accelerator Research Organization (KEK), 2006

KEK Reports are available from:

Information Resources Division
High Energy Accelerator Research Organization (KEK)
1-1 Oho, Tsukuba-shi
Ibaraki-ken, 305-0801
JAPAN

Phone: +81-29-864-5137
Fax: +81-29-864-4604
E-mail: irdpub@mail.kek.jp
Internet: <http://www.kek.jp>

Stainless-steel X-band High Power RF Load with Low Surface Field

A. Lounine¹, T. Higo, N. Kudo and K. Watanabe²

KEK, High Energy Accelerator Research Organization
1-1, Oho, Tsukuba, Ibaraki, 305-0801, Japan

² The Graduate University for Advanced Studies, Hayama, Japan.

Abstract

Stainless-steel high power X-band RF loads proposed at SLAC in 1995 have been in operation for many years at SLAC for linear collider test facility. In this paper we describe the improvements of this load structure with reducing surface electric field. We present a unique designing process and the optimized design. Especially the distribution of maximum surface electric fields along the lossy section of the load was designed uniform in addition to making the edges of all lossy cells rounded. The optimization of the load parameters was performed by dividing the lossy section into a series of simple constituent cells and treating these cells with S-matrix formalism. A new elliptical polarizer was also proposed in which a smooth transition is realized between linearly polarized part and the circularly polarized part. This polarizer design prevents local enhancements of the electromagnetic field at this transformer and makes the bandwidth of the load as broad as 800MHz below -20dB. Finally the present design features were confirmed experimentally in low power measurement during fabrication. It was tested in high power up to 70MW with 200ns and 55MW with 400 nsec, both limited not by the present load but by the test system. It was confirmed that the lossy property of the magnetic stainless-steel material was reduced by a high temperature brazing process but the reduction of the volume resistance is by a factor of 1.5, in which we can still design compact loads using it.

¹ Present address: PSI, Switzerland, e-mail: andrei.lounine@psi.ch.

1. Introduction

The X-band technology is one of the most promising candidates for the compact particle accelerators especially those based on high-gradient acceleration. This idea is realized when the high RF power is reliably treated by overcoming the difficulties related to its short wavelength. Then we can make the RF components of the accelerators more compact and less expensive. The high power RF load is one of the key components of such accelerators. Such an accelerator consists of the high power RF loads at several places; for example, the output from the traveling wave accelerator structure, the various places in the pulse compression system or the power dividing section and the loads for the RF sources in the testing stage. Typical parameters of these loads for linear collider use [1], for example, are 100 MW peak power, 400 nsec pulse width and repetition rate of 50 Hz or more.

Water loads are used sometimes as high power dummy. However, the fear of breaking ceramic window separating between vacuum and water made us design the dry load. High power dry loads using bunch of SiC buttons are used at a few tens of MW level at S-band[2] and C-band[3] application, which uses conduction heat transfer. We might think to apply this idea to the high frequency load such as at X-band. However, high peak power of 100MW level especially used for high energy accelerators makes electric field very high in high-frequency small-size components. Therefore, we took the idea of using the metallic surface to directly absorb the electromagnetic power. The magnetic stainless steel was used for this purpose. There are a variety of loads based on this idea. Some examples are such as a simple tapering of the rectangular WR90 wave guide[4], WR90 waveguide with inserting multiple plate in the waveguide as absorber[5], bunch of lossy cells comprising of a pair of grooves in its cylindrical waveguide surface transmitting TE₁₁/TM₁₁ dipole mode[6] and coaxial configuration with its lossy inner conductor with bunch of disks transmitting TE₀₁ mode[7].

As described above, a compact RF load design by S. Tantawi et al. of SLAC exists [6]. It uses the circularly polarized TE₁₁ mode in the lossy section of the load, which is made of magnetic stainless steel. The mechanism of the load is the power dissipation along a stack of self-matched cells made of lossy metal. To make the time-averaged electromagnetic field azimuthally uniform, the linearly-polarized TE₁₀ mode in a rectangular wave guide is converted to the circular-polarized TE₁₁ mode before entering into the stack of lossy load cells.

Many loads of the design were made and used at SLAC in high power [8, 9]. One of the speculations which limit the high power capability of the load is the RF breakdown or arcing caused by a high electric field on the surface. This is observed especially in the lossy load stack area [10, 11]. The initial design of the load was done with semi-analytical approach, which has to assume sharp edges in each load block with choke geometries [6] (See Fig.1). Even the natural rounding of R0.38 mm specified in the mechanical fabrication of cells on the sharp edges gives a severe field rise. Therefore, the edges are intentionally rounded to be R2 mm in the present design. In order to further reduce the maximum surface electric field, the present load was designed to make the strength of electric field uniform among all of the lossy cells rather than making the heat dissipation uniform. Further optimization of this idea was done with designing a proper choice of a distance between individual cells and taking a proper position of the end screen.

The overall band of matching of the SLAC original design is limited mainly by the passband of the pin type TE_{11} mode polarizer. We proposed here a new design, a smooth elliptical polarizer, for further suppressing the field and expanding the load band width.

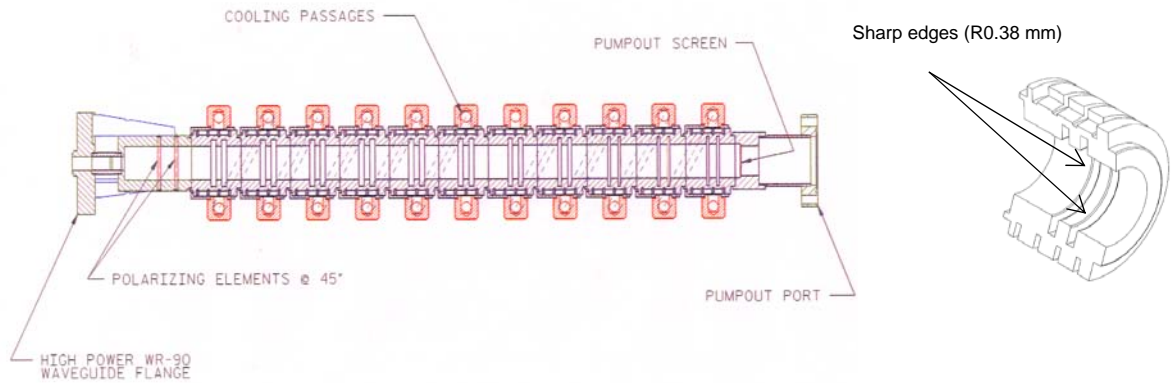


Fig.1 Schematic of original SLAC compact dry RF load design

In the present paper, the design strategy and the theoretical base are described in Sec. 2. Results of the simulation on the lossy section and the elliptical polarizer using S-matrix formalism are presented in Sec. 3. The change of the load material properties due to high temperature treatment in the fabrication is presented in Sec. 4. Then we confirmed the present simulations with the cold measurements as shown in Sec. 5. Finally the high power performance was briefly described in Sec. 6.

2. Theory

Load design

The basic structure of the proposed RF load is shown on Fig. 2. RF power dissipates sequentially in pairs of chokes placed in a circular waveguide. Each pair of chokes forms a lossy cell. The dissipation is a result of losses due to the resonance of TM_{11} -like mode in each cell. At the end of the load is located a short which reflects back the RF power. Thus the field distribution inside a cell depends on the amplitude and phase of incident and reflected waves and cell geometry itself, such as shown in Fig. 3.

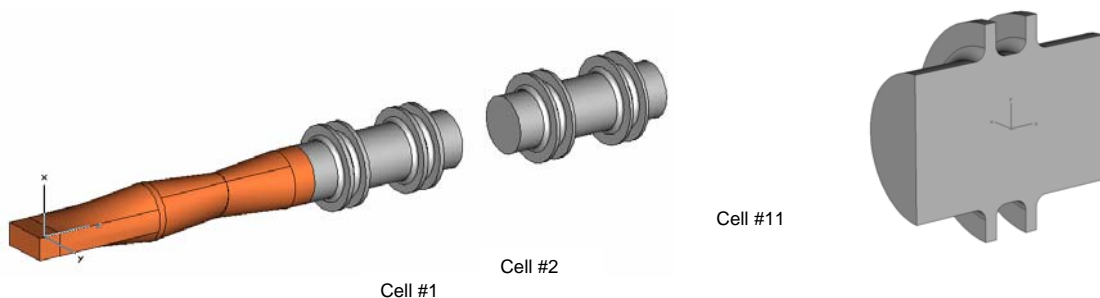


Fig. 2 Schematic of the present RF load.

The geometry of cells (choke width) changes gradually along the load in order to increase the power dissipation ratio. At the same time we keep the surface electrical field uniform. The last cell has the narrowest separation between a pair of chokes and hence a smallest internal volume. So it is obvious that with the same absolute amount of dissipated power the maximum field will be higher in the last cell than in the first. Thus to correct this dependence we have to raise the dissipation of upstream cells. Let's define the geometry factor of the cell k_g^i as

$$k_g^i = \frac{P_i}{P_N},$$

where $i = 1..N$ – the cell number, P_i – power dissipated in i -th cell, N – the number of cells in the load.

The process of finding proper geometry factors can be performed iteratively starting from the linear function: $k_g^i = 2^{i-1}..1^{i=N}$. Because the phase of reflected wave is unknown we assume the worst case that an overall field distribution in the cell is the scalar sum of the amplitudes of the incoming wave and the reflected one. Then we can write a set of equations as follows.

$$(1 - A_j) \prod_{i=1}^N A_i \left[\frac{1}{\prod_{i=j}^N A_i} + \frac{\prod_{i=j}^N A_i}{A_j} \right] = k_g^j / k_{sum},$$

where $j = 1..N$, $k_{sum} = \sum_{i=0}^N k_g^i$, $A_i = 10^{-\frac{X_i}{10}}$ and X_i – attenuation of i -th cell in dB.

This system can be solved numerically and the attenuation of individual cell A_i is obtained. Then actual cell parameters, the groove width, the groove width and the groove separation, are optimized by using a multi-parametric optimization algorithm [12]. In this optimization process, the actual electromagnetic field and the matching for any set of cell parameters are computed by HFSS. The diameter of the circular waveguide is fixed for the present optimization. The optimization was performed to keep the matching condition and to obtain the defined attenuation of individual cells.

An example of cell calculation in Fig.3 illustrates that an inphase cell excitation gives significantly lower maximum electrical field comparing to $\pi/2$ phase shift case. Thus after defining geometries of cells we have to find proper distances between them and position of short screen so that incident and reflected waves should always excite any cell in either inphase or antiphase condition. This will give us further reduction of maximum surface electric field.

At the next iteration step the geometry factors k_g^i of cells are refined according to actual values of calculated surface electric field, smaller k_g^i gives less electric field. The process is repeated until the distribution of electric field along the load becomes uniform.

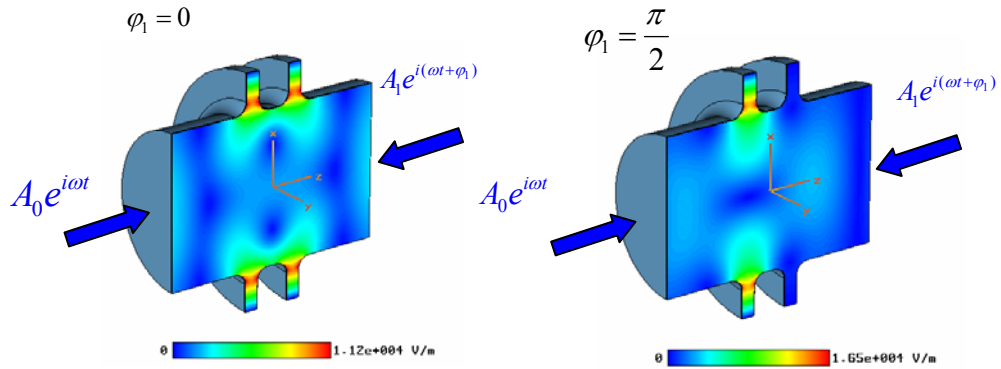


Fig. 3. Electrical field distribution inside cell depending on relative phase between incident wave and reflected one.

Polarizer design

The lossy section of the load is operated in a circularly polarized TE_{11} mode. A scheme of the smooth elliptical polarizer is shown on Fig.6. The polarizer consists of three parts - a smooth rectangular to circular junction and a pair of identical smooth circular to elliptical transitions. The first part of polarizer transforms the TE_{10} mode of rectangular waveguide to a linearly polarized TE_{11} mode of circular waveguide. The axis of the elliptical cross section in the following rotator is rotated by 45° with respect to the incident RF electric polarization in TE_{11} mode. This linearly polarized TE_{11} mode wave can be considered as the superposition of two orthogonal, in-phase, linearly polarized TE_{11} waves, one of which is oriented normal to the long radius of the ellipse whereas the other one to the short. These two TE_{11} waves have different propagation constants when passing through the polarizer. The transition length between the circular position and the elliptical position is chosen to minimize reflections and also to provide a phase shift of 45° each, 90° in total.

Finally two TE_{11} mode components, orthogonal with each other and 90° apart in time, recombine as a circularly polarized wave at the output of the polarizer. The reduction of maximum electric and magnetic fields with respect to those of the linearly polarized TE_{11} wave is a factor $1/\sqrt{2}$.

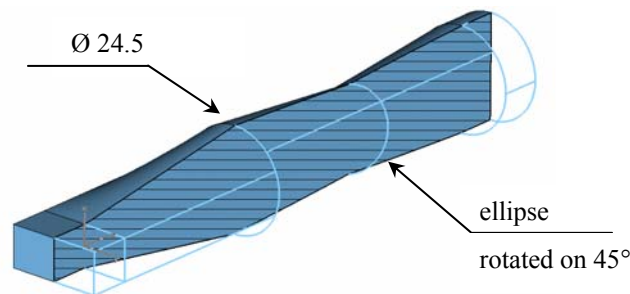


Fig. 6. Schematic view of the TE_{11} mode smooth elliptical polarizer.

Moreover polarizer doubles the effective length of RF power dissipation in a load because the symmetry plane of incident linear polarized TE_{11} wave is rotated by 90° each time when signal propagates through the load and comes back to the polarizer and thus the backward wave is completely reflected by the rectangular junction for the first

reflected wave. Therefore RF signal have to pass four times through the load until linearly polarized TE_{11} wave will restore its initial polarization and comes out of the load as a reflected wave.

3. Simulations

General approach

The load as a whole is a complicate RF structure with a size of order of tens wavelength. Therefore, it is not practical to realistically simulate it, especially in 3D, as a single unit. One of the remedies is to split the complex structure and treat it as an ensemble of elemental RF elements [13]. Each RF element is described by its own scattering S-matrix and the overall S-matrix of the load can be obtained by cascading all of them. The concept of load decomposition is schematically shown in Fig.7. The load consists of the upstream polarizer and a stack of 11 lossy cells terminated by a short. Constant cross sectional wave guides are inserted between elements.

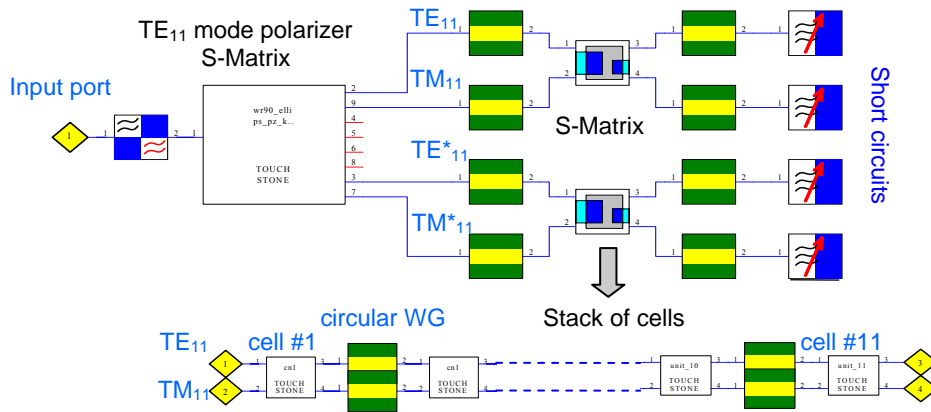


Fig.7 Schematic drawing of load decomposition into elements.

Polarizer

Figure 8 shows the performance comparison between two types of TE_{11} mode polarizers, pin-type and smooth elliptical type. Despite the fact that the elliptical polarizer is more complicated and less compact, the wider passband and higher polarization efficiency make it an attractive choice for the RF load design.

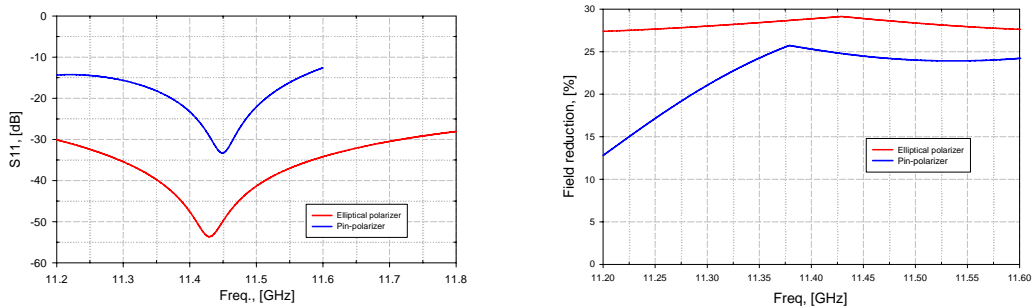


Fig. 8 Comparison of two types of TE_{11} mode polarizer, pin-type and smooth elliptical type.

Because the circular to elliptical transition works as a reflector for a certain kind of RF modes, the present polarizer was optimized to eliminate possible resonances within working frequency band. The nearest trapped modes are shown on Fig. 9. These are not harmful because the frequencies are away from the operation frequency, 11.4GHz, by more than the Q width.

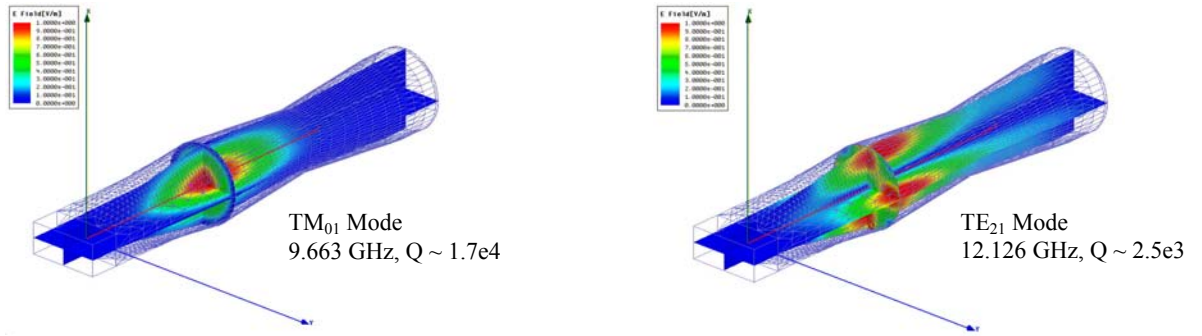


Fig. 9 Trapped modes inside elliptical polarizer.

Stack of lossy cells

The reflection and transmission properties of each lossy cell are shown in Fig.10. A pair of cells, #1 and #2, and another one, #3 and #4, can be designed identical, respectively, without sacrificing the overall property. The dependencies of losses versus frequency for each cell were additionally optimized to spread the total power dissipation uniformly inside the load passband. The equivalent conductivity of the stainless steel was taken from experiment equal to $1.5e5 \text{ (Ohm}^{-1}\text{m}^{-1}\text{)}$.

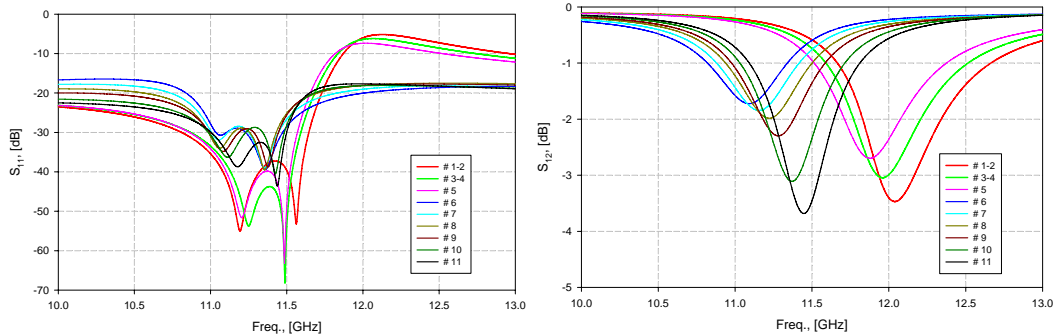


Fig. 10 Modeling result of each lossy cell.

Phasing of lossy cells

The proper phasing between incident wave and the reflected wave is important to suppress the field enhancement within each cell. Since the ratio of amplitudes of incident and reflected wave is reduced upstream of the load, it is practically necessary only for the last few cells. Therefore, we tuned the last four cells where the field enhancement due to reflection signal is higher than 10 %.

The scheme shown in Fig.11 features the process of phase tuning for the last cell. The phase of incident wave is set to zero while the phase of reflected wave is defined using ideal directional couplers. The proper phase shift is given by choosing the position of a short screen terminating the load.

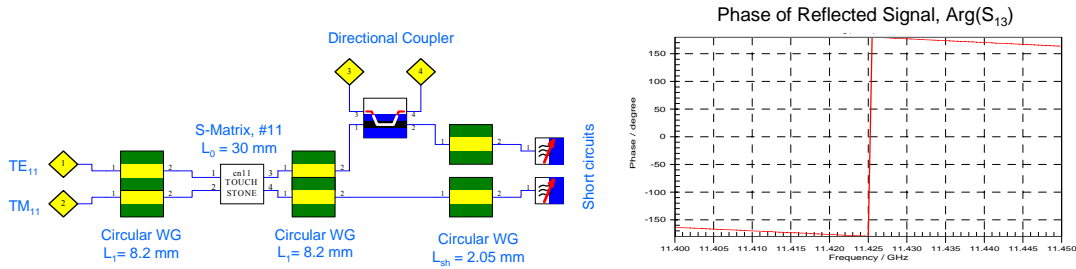


Fig. 11 Scheme of the last cell phase tuning.

The maximum values of surface electric field distribution along the load before and after this phase tuning is shown in Fig. 12. Since the variation of surface electric fields exceeded 50% after the phase tuning, we proceeded with the next iteration of the design.

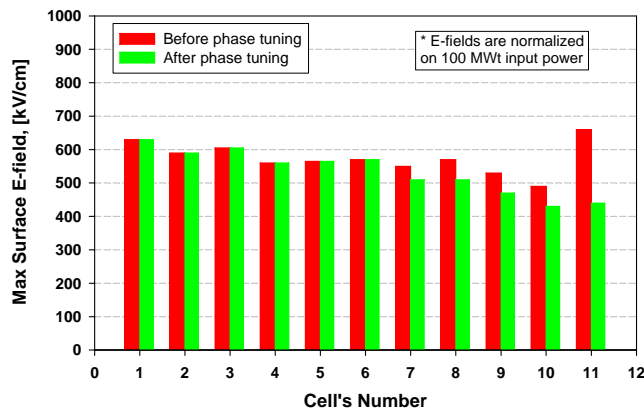


Fig. 12 Phase tuning of the last cell showing the distributions of maximum surface electric fields at each lossy cell, red for before tuning and green after.

The final results of a new load simulations and a comparison with original SLAC design are presented in Fig.13. The one pass attenuation through the load is about 14 dB at 11.4GHz. The reflection over the bandwidth of 1GHz is below -20 dB. The frequency response of the reflection from the load follows almost the reflection of elliptic polarizer. This means that all RF power entered to the load is very effectively dissipated inside. Thus we found the optimum configuration of the RF load in a given frequency band. At the same time the maximum value of surface electric field was decreased for 40% comparing to original SLAC design.

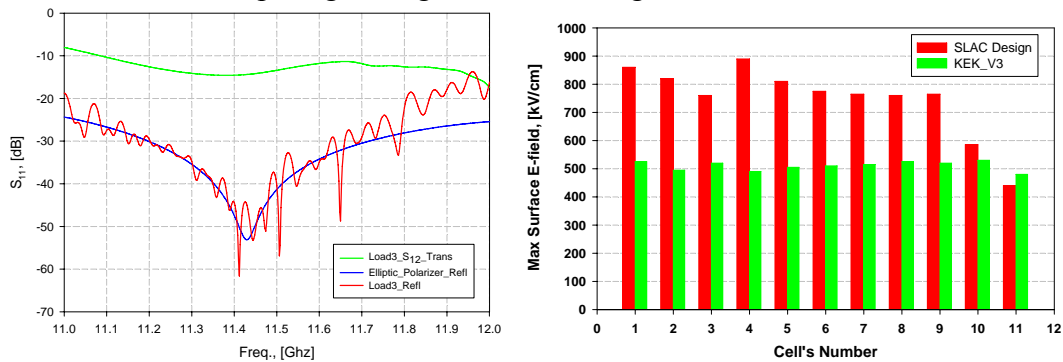


Fig. 13 Results of the optimized RF load performance.

Tolerances

The tolerance of lossy cells was estimated. Three main parameters of lossy cells were varied and calculated the reflection from the load as a whole. The three parameters are the width “t”, depth “r” of the grooves and the separation “s” between a pair of them. The result is shown in Fig.14. Fifty microns (50 μm) deviations of the basic parameters still give an acceptable reflection level from the load. Therefore, this value can be referred as the general tolerance value.

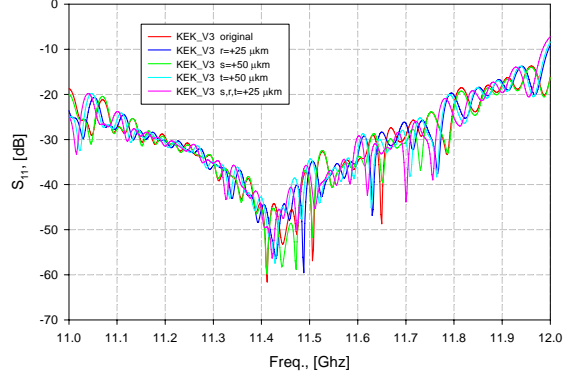


Fig. 14 Reflection from load varying various dimensions to estimate the tolerance.

Consideration of pulse heating

At last we calculated the effect of the pulse RF heating [14]. High surface magnetic field results in the material surface heating during each RF pulse. Many cycles of them could cause the surface destruction leading to RF discharges and arcings. We estimate it with the last cell #11 because it is most critical there. The computed distribution of surface magnetic field is shown in Fig.15a. The RF heating of a metal surface was calculated with a simple 1D model [15]. The maximum pulse temperature rise ΔT is estimated by :

$$\Delta T = \frac{R_s H_{||}^2 \tau}{(2\delta + \sqrt{\pi\alpha_d\tau}) \rho c_\varepsilon},$$

where $R_s = 1/(\sigma\delta)$ is the surface resistance, σ is the electrical conductivity, δ is the skin depth, $\alpha_d = k / \rho c_\varepsilon$ is thermal diffusivity, k is the thermal conductivity of the metal, ρ is the density, c_ε is the specific heat and τ is the duration of RF pulse.

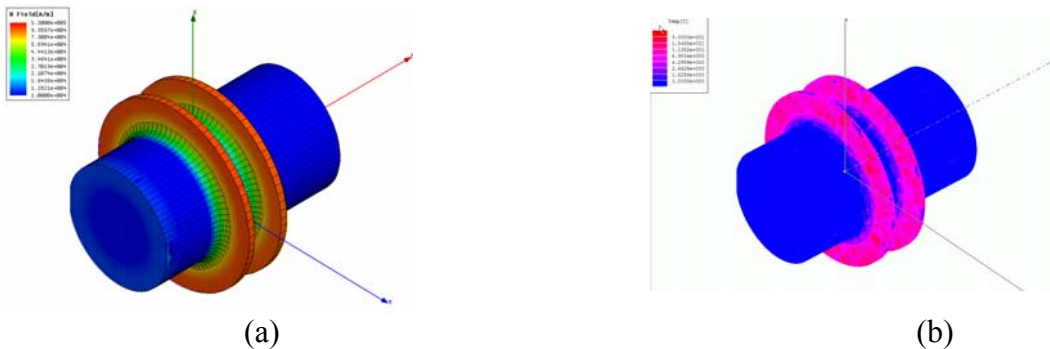


Fig. 15 (a) Magnetic field at cell #11 under input power of 100 MW, 400ns into the present load. (b) The resultant surface temperature rise with highest at 31°C.

For a given input RF power, 100 MW and 400 ns, into the load the maximum value of a tangential surface magnetic field H_{\parallel} is 120 kA/m and the corresponding temperature rise is about 31°C. The result of a temperature rise distribution calculated with a full 3D code Ansoft ePhysics [16] is shown in Fig. 15b. The maximum growth of surface temperature is about 30°C as well. This value is considerably lower than a critical temperature of 200°C which causes a damage of stainless steel material [17].

4. Change of lossy property during fabrication

Material property change

The curie temperature of ferrite stainless-steel, SUS430 with 17% Cr, is 700°C [19]. Therefore, the lossy properties of magnetic stainless may change due to the thermal cycle for brazing. Since the actual manufacturing process takes three stages of brazing at 1000°C or higher, as described in Sec. 5, we prepared a test cell, equivalent to the first cell #1, to study the lossy properties when heated at 1100°C.

Test cells were fabricated to study the material change due to the high temperature heat treatment on the magnetic stainless steel. The dimensions of cell #5 were taken for all of the test cells. The transmission property through the cell was measured to estimate the lossy property of the material. The results were shown for those before, after the first and after the second firing at different temperatures. The effect of the initial heat treatment at 1100°C is most severe. The following treatments at lower temperature or even at the same temperature were found not as sensitive as the initial one. The resistance as of completion became less than the original one by a factor 1.5.

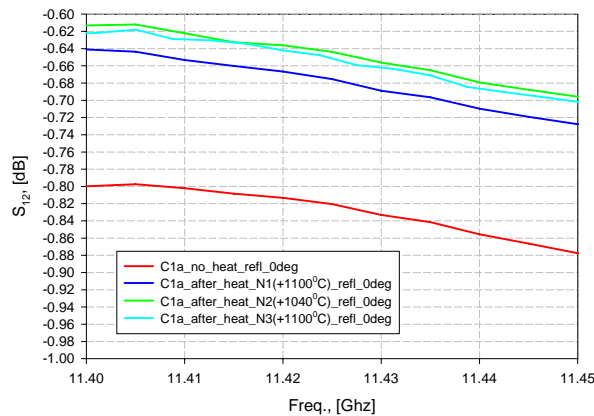


Fig. 16 Change of the attenuation through a cell due to thermal treatment

The change of the lossy property was also confirmed with the actual eleven cell stack. The one-way attenuations of lossy eleven cell stack before and after brazing were shown in Fig. 17. The calculated values are also plotted in the same figure assuming the conductivity of $1.85e5$ ($\text{Ohm}^{-1}\text{m}^{-1}$), about 50% higher than original one, the same as that observed in a single-cell measurement. With this lossy property, the one-way attenuation at working frequency was as much as 13 dB, resulting in the total attenuation within the load until the power reflecting back from load 52dB, big enough in a practical sense. Therefore, the amount of the degradation of lossy property due to

high temperature heating processes is still within an acceptable level to make the present RF load.

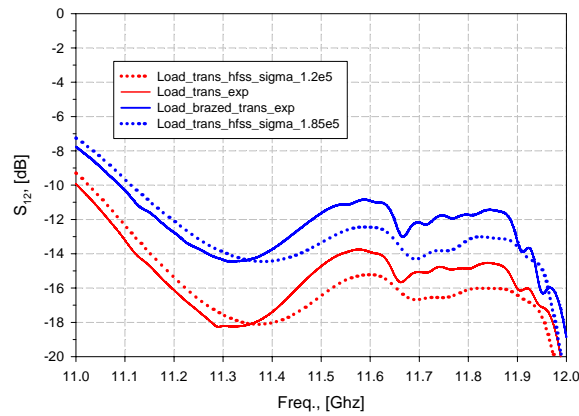


Fig. 17 One way transmission of an actual stack of lossy cells, #1-11. Dotted lines are obtained from simulation assuming the conductivity of $1.2e5$ (red line) and $1.85e5$ (blue line) ($\text{Ohm}^{-1}\text{m}^{-1}$), respectively. Solid lines are those measured, as of machined parts (red) and as of brazed (blue).

For further information, the temperature dependence of the degradation of the lossy property was evaluated. It was performed by measuring the insertion loss of the system of the present load configuration but with only a load cell which was terminated by a shorting plate. The load cells are heat-treated at various temperatures from 600°C to 1100°C . The insertion loss was evaluated as an average value between 11.05 and 11.1GHz.

Taking this test results into account, the information was summarized as below.

1. The loss degradation occurs above 600°C .
2. The amount of degradation does not vary much between 750°C and 1100°C .
3. The lossy property stays constant by further high-temperature treatment at lower temperature once treated at high temperature at 1100°C .

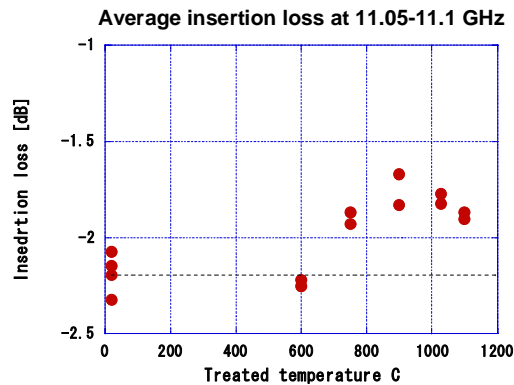


Fig. 18 Return loss with the cells #5 which are heat-treated at several different temperatures.

5. Fabrication and low-power measurement

Fabrication process

Because of the time limitation we started the actual load manufacturing before completing the optimization. The RF load presently fabricated by KEK is based on the result after the second iteration. The lengths of cells are set equal and fixed. Parts such as the polarizer elements and the actual lossy cell are shown in Fig. 19. Using these parts, the fabrication process consists of three steps as listed below.

1. Polarizer part fabrication

- a) Polarizer parts are made of oxygen-free copper. The shaping is made by milling and by wire electric discharge machine. These parts are cleaned by chemically polished.
- b) These parts are brazed with gold-copper alloy at a temperature about 1040°C.

2. Lossy stainless steel part fabrication

- a) Lossy magnetic stainless steel parts are made by turning lathe. The surface was cleaned by chemical polishing SUSpika [20].
- b) These parts are brazed to form a stack of lossy cells. This brazing is done with copper metal at 1100°C.
- c) Water cooling jackets are brazed on lossy cells with gold(25%)-copper(75%) alloy at a temperature about 1040°C.

3. Final assembly

- a) All sub-assembled parts are brazed with gold(35%)-copper(65%) alloy at around 1000°C.
- b) Vacuum pumping port flange is TiG-welded.



Fig. 19 Parts for the present RF load. Left: three parts for a polarizer. Right: lossy cell.

Polarizer

To confirm the transmission characteristics of the lossy cells, two elliptic TE_{11} mode circular polarizers were made. Figure 20 shows both the calculated and measured reflection coefficient from the two polarizers connected one to another. The agreement is good enough for the present purpose.

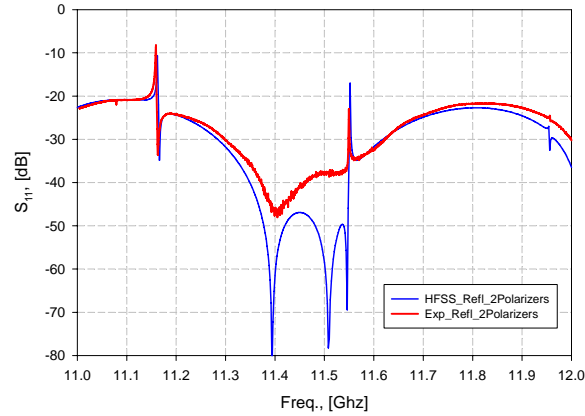


Fig. 20 The reflection coefficient from two polarizers in a configuration facing with each other

Cell attenuation measurement

An experimental study on the material properties of various lossy materials shows the surface resistance of the stainless steel SS430 to be 19 times higher than that of copper. This is equivalent to the conductivity of $1.6e5 \text{ (Ohm}^{-1}\text{m}^{-1}\text{)}$ [18].

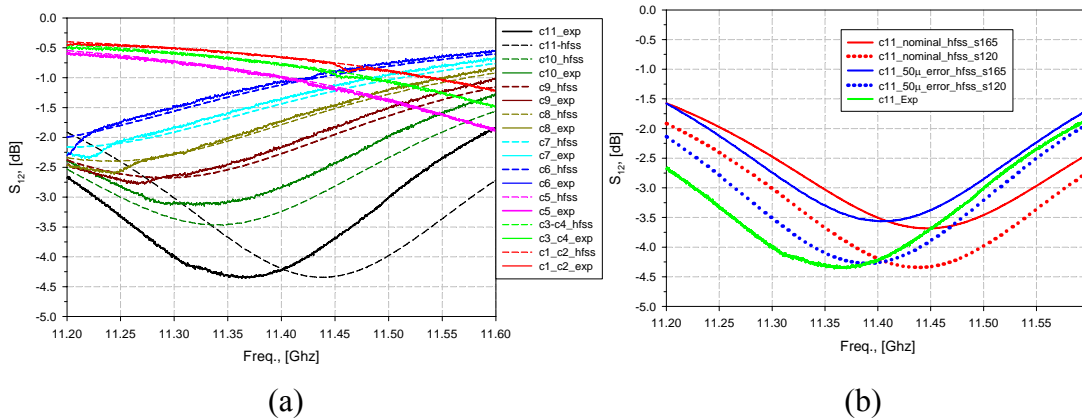


Fig. 20 a) The attenuation through a cell, measured and calculated, b) The attenuation through a cell #11, Red: nominal geometry, Blue: geometry with $50\mu\text{m}$ errors, Solid: nominal conductance $1.6e5 \text{ (Ohm}^{-1}\text{m}^{-1}\text{)}$, Dotted: measured one $1.2e5 \text{ (Ohm}^{-1}\text{m}^{-1}\text{)}$, Green: experiment.

We performed the evaluation of the material loss characteristics using the cells for the actual load. The results of measurements of cells attenuation before brazing are shown in Fig. 20(a) along with calculated ones. The equivalent conductivity of stainless steel was assumed to be equal $1.2e5 \text{ (Ohm}^{-1}\text{m}^{-1}\text{)}$ for the calculation. We can not clearly identify the reason of the difference between these two values. Probably it is a result of a heat treatment during the manufacturing process of a test cell. In this paper, we take the value of $1.6e5 \text{ (Ohm}^{-1}\text{m}^{-1}\text{)}$ for the initial optimization of the load. The most sensitive behavior due to a possible geometry errors is demonstrated by cells #10-11. The differences between calculations and experimental results can be explained by

mechanical tolerance of 50 μm . The detail analysis of cell #11 behavior depending on fabrication tolerances and conductance of a stainless steel is shown in Fig. 20(b).

Whole assembly

Finally the stack of lossy cells was brazed with polarizer and short screen. The measured reflection signal of the whole load and calculated one are shown in Fig. 21. Both curves are very close. The measured frequency band with level of reflection below -20 dB is about 1 GHz which is the same as predicted by simulations

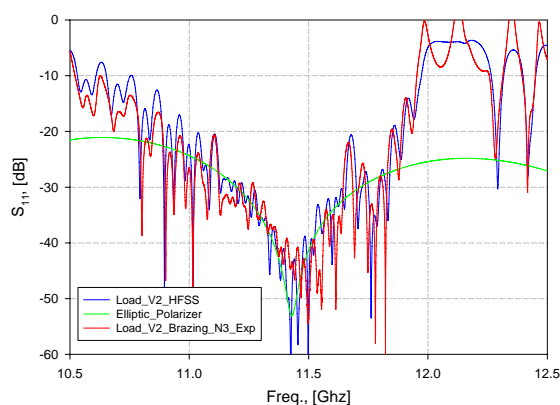


Fig. 21 Matching properties of the completed load. Red: experimental, blue: HFSS calculation and green: polarizer with matched load behind.

6. High power performance

Test setup

High power performance was evaluated at XTF of KEK [11]. The actual setup is shown in Fig. 22. The power was fed from the top to the present load. The vacuum is evacuated by an ion pump at the bottom and that through the wave guide ion pumps.

The processing was performed up to the RF pulse length of 400ns at the pulse repetition rate of 50Hz within about 60 hours. However, several straight waveguides cleaned in different manners were inserted as a study in parallel to the load processing and most of the processing period was served for the conditioning of such waveguide components, meaning that the processing time needed for the load itself should be much shorter than 60 hours. The power trend was shown in Fig. 23. The first two arrows show the timing when we replaced the bad waveguide by standard good ones. The last arrow shows the end of the processing limited by breakdowns in the WR90 waveguide system in the upstream side.

Observations

The RF pulse shape incident to and reflected from the present load was monitored. Acoustic sensors (Piezo device) were attached on the surface of the load so that any thermal shock was measured as the acoustic emissions to identify the position and the strength of the energy deposit. The thermal shock of the pulse serves as the normalization of each sensor, which is proportional to the RF pulse energy. A photo-multiplier tube monitors any light inside the load through a view port attached on the H-bend located at the top.

When big breakdown happens inside the load, the abrupt increase of the acoustic emission was measured upstream of a certain position of the load while the decrease at the downstream of the same position. Typical example is shown in Fig. 24. This example shows the position of the big breakdowns at around number #5 where RF power is reflected. Frequently the light emission was accompanied.

Comparison of two loads

The distributions of the breakdowns in the present KEK-design load were compared with that of the load of SLAC design. Fig. 25 shows the population of breakdowns in both structures, the test for SLAC-design was at higher than 50MW input for 20 hours while that of the KEK-design was higher than 55MW for 5 hours. It was found that the number of breakdowns per hour is roughly one per hour, the same with both cases, though at a higher power for the test of KEK one so that the breakdown rate seems lower in KEK one. Also to be noted is that the breakdown at the mode converter was clearly suppressed. It was found that the breakdowns at the upstream side of the lossy cells still frequently happened. This behavior is consistent to the calculated field distribution along the present version of the load which is shown in Fig. 26. Note that the present fabrication was not based on the final optimized parameters but that picked at the second iteration. Even if the surface electric fields at the upstream of the lossy cells are reduced compared to the original SLAC design, it is still high to cause breakdowns at least during initial processing of the load.

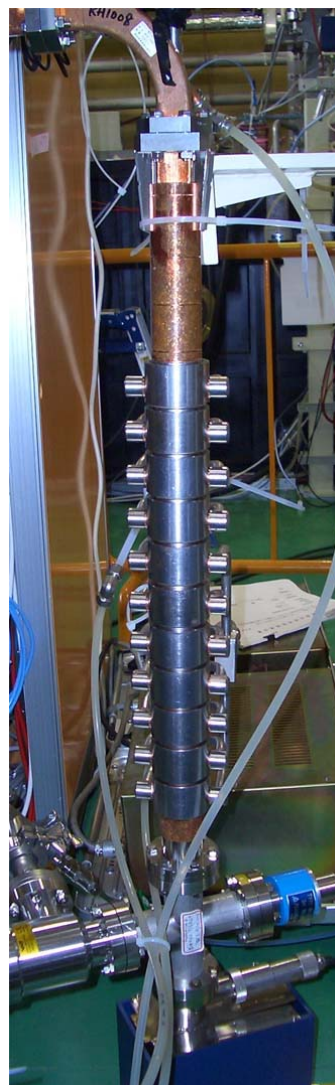


Fig. 22
High power test setup.

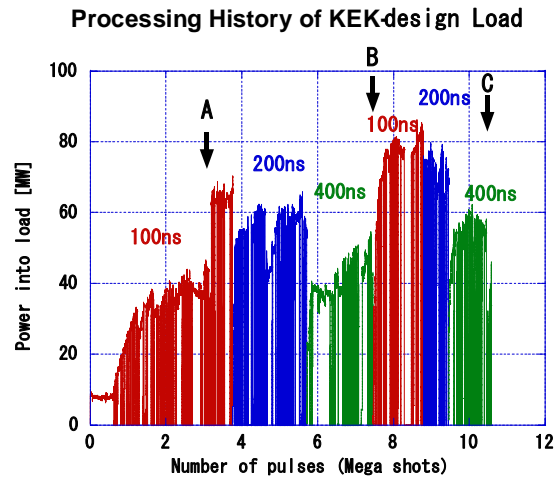


Fig. 23 High power processing history of the present load.

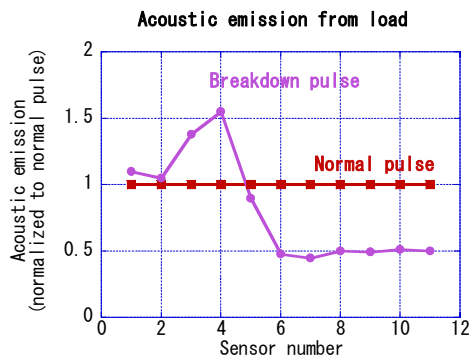


Fig. 24 Acoustic signal amplitude for breakdown event normalized by the normal event.

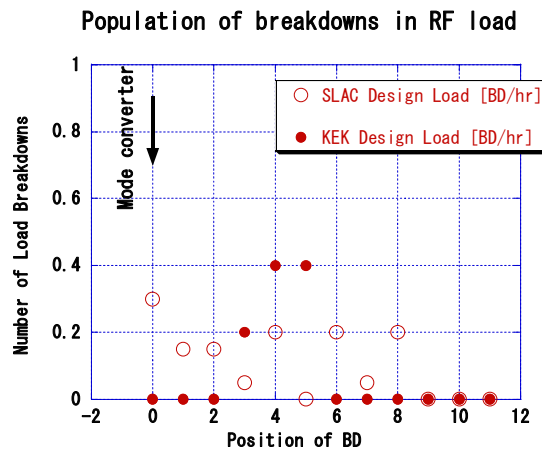


Fig. 25 Breakdown population in high power operation for two types of RF loads. The statistics was obtained on SLAC load above 50MW for 20 hours, while that of KEK load above 55MW for 5 hours. The load cell numbering is from upstream (#1) to downstream (#11).

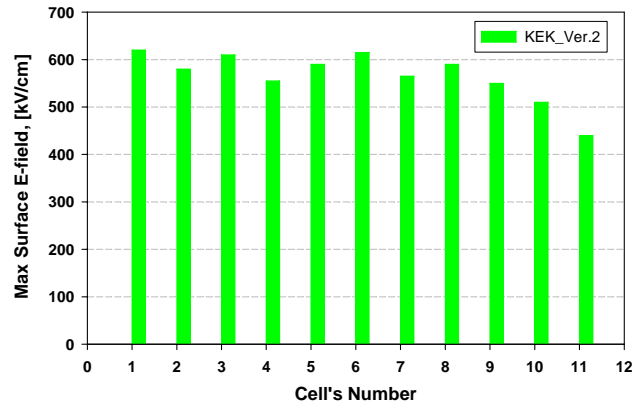


Fig. 26 Calculated distribution of maximum surface electric fields at each lossy cell along the fabricated RF load. The fields are normalized at 100 MW input power.

7. Summary and conclusion

A new design for the high power RF dry load was performed inspired by the SLAC load design[6]. A treatment of the whole load with S-matrix formalism was developed and used for the optimization of the parameters. The mode conversion was performed by a smooth transition so that the overall matching bandwidth below -20dB became as wide as 800MHz. The load is designed to be made of the magnetic stainless steel. The lossy property of the material changes due to the high temperature fabrication processes was confirmed not significant. The equivalent volume resistance was measured to decrease at 11.4GHz by a factor of 1.5.

An actual load was fabricated based on the present design. It was proved that it can be operated at 50Hz stably up to 70MW for 200nsec pulses and 55MW for 400nsec pulses. Though this is below our goal of 100MW, the limitation is not due to the load but due to the power handling capability of the present test system. The present load showed better performance especially in the mode converter section than that of SLAC design.

Acknowledgment

The authors greatly thank Dr. S. Tantawi of SLAC for the valuable discussion related to the design and performance. They also thank Dr. S. Kazakov of KEK for helpful discussions through the design process.

References

1. ISG Study Report, KEK-Report 2000-07, SLAC R-559.
2. H. Matsumoto et al., "Experience on the High-Power SiC Microwave Dummy-Load Using SiC Absorber", Proc. 1999 Particle Accelerator Conference, PAC99, New York, 1999.

3. T. Sugimura et al., "Development of C-band dummy load and 3dB hybrid for Super-KEKB", Proc. 28th Linear Accelerator Meeting in Japan, 2003, in Japanese.
4. Mainly used as loads at medium power of a few tens of MW level at KEK X-band facility.
5. Supplied by BINP, Protvino, and used at KEK from mid 1990's.
6. S. G. Tantawi and A. E. Vlieks, "Compact X-band High Power Load Using Magnetic Stainless Steel", Proc. 1995 Particle Accelerator Conf., p. 2132.
7. Z. D. Farkas, "TE01 High Power Disk Loaded Guide Load", SLAC-TN-04-075, February 2005.
8. D. Schultz, C. Adolphsen, D. Burke et al., "Status of a Linac RF Unit Demonstration for the NLC/GLC X-band Linear Collider", Proc. 9-th European Particle Accelerator Conference, EPAC'04, Lucerne, 5-9 July, 2004
9. W.R. Fowkes, E.N. Jongewaard, R.J. Loewen, S.G. Tantawi and A.E. Vlieks, "An All-Metal High Power Circularly Polarized X-Band RF Load", Proc. 1997 Particle Accelerator Conf., Vancouver, Canada 12-16 May 1997
10. Marc Ross, private communication.
11. K. Watanabe et al., "X-band High Power Component Study for High Gradient RF LINAC", Proc. of the 2nd Japanese Accelerator Society Conference, 2005, Saga, Japan.
12. R.HOOKE, T.A.JEEVS, "Direct search solution of numerical and statistical problems", Journ. Ass. Comput. Mech., 8, 1961.
13. B.S. Perlman and V.G. Gelnovath, "Computer Aided Design, Simulation and Optimization" in Advances in Microwaves, L. Yang and H. Sobol Eds., Vol. 8, New York Academic Press, 1974.
14. D.P. Pritzkau, et al., "Possible High Power Limitations From RF Pulsed Heating", 4th RF Workshop (RF98), Watsonville, California, October 1998. SLAC-PUB-8013.
15. D.P. Pritzkau, "RF Pulsed Heating," SLAC-Report-577, Ph.D. Dissertation, Stanford University, 2001.
16. <http://www.ansoft.com/products/tools/ephysics/>
17. O.A. Nezhevenko, "On the Limitations of Accelerating Gradient in Linear Colliders Due to the Pulsed Heating," PAC97, Vancouver 1997, p.3013.
18. H. Sakai et al., "Measurement of the surface resistance of iron, stainless steel and Kanthal at 3~16GHz range", JLC-NOTE No.40, 1993, in Japanese.
19. "Stainless steel", Page 577, Kinzoku-binran, 5th issue, Maruzen, Japan, 1990.
20. "SUSpica", Stainless steel cleaning method, San-ai plant co.